Development of Algorithm for Newtonian Compressible Fluid Flow Based on Finite Element Method

Fatima A. Mohammed, Alaa Al-Muslimawi*, Reisan Y. Yasir

Department of Mathematics, College of Science, University of Basrah, Basra, Iraq

*Corresponding author E-mail: alaa.abdullah@uobasrah.edu.iq

Doi:10.29072/basjs.2021302

Abstract

In this article, we present the numerical investigation for compressible Newtonian flow in two dimensional axisymmetric channel. Galerkin finite element method is applied to accommodate compressible and incompressible flows. A continuity equation and time-dependent conservation of momentum equations are used to describe the motion of the fluid, which are maintained in the cylindrical coordinate system (axisymmetric). To meet the method analysis, Poiseuille flow along a circular channel under an isothermal state is used as a simple test problem. This test is conducted by taking a circular section of the pipe. Comparision between compressible and incompressible results in terms of convergence has been conducted for axial velocity and pressure. Findings reveal that, convergence-rates of velocity and pressure is faster an incompressible case compared to compressible. In addition, the level of velocity convergence is higher than pressure for both compressible and incompressible. Moreover, the low level of Mach number demonstrates that piecewise-constant density interpolation is equitable to linear density interpolation

Article inf.

Received:
19/10/2021

Accepted:
18/11/2021

Published:
31/12/2021

Keywords:

Compressible fluid flow, Galerkin finite element method (GFEM), Newtonian flow, Numerical methods.

1. Introduction

In this study, numereical investigation of compressible Newtonian laminar flow is conducted based a Galerkin finite element ($GFEM$) method. Here, compressible Newtonian equations are expressed as a combination of two differential equations; called continuity and time-dependent conservation of momentum equations. These equations are presented in this study in cylindrical coordinate system (Axisymmetric flow) (for more details see [1]). Particularly, the effects of compressibility occur in both gases and liquids through the variation of density. Density itself depends on temperature, pressure and concentration levels of fluids [2]. Flows of liquid materials, at moderate pressure levels, can be considered as incompressible. Nevertheless, at large pressure-differences, such flows may display some mild compressibility effects. Mach number, the ratio of fluid velocity to the speed of sound (Ma =u/c), characterizes the influence of compressibility on a flow field [3-4]. Flows at low Mach number may be described as incompressible, whilst for those at moderate to high Mach number, compressibility effects will be prominent. Recently, compressibility plays an important role in some applications such as: steam turbine, polymer extrusion, injection molding with polymer melts and exploration of petroleum (for more details see [5-8]). Moreover, in capillary rheometry, compressibility may have a significant influence on features such as the time-dependent pressure changes within a system (see piston-driven flows [9]). Extensive literature studies on the computational solution of flows that manifest compressibility effects have been conducted. In this context, the finite element method played essential role for solving various problems. Under this method, different techniques have appeared such as Streamline-Upwind/Petrov-Galerkin (SUPG) algorithm, Galerkin Least-Square (GLS) and Taylor-Galerkin/ pressure-correction scheme (TGPCM) [10-11]. In this context, one can see various investigations of the compressible flows that have been conducted based on finite element methods. In addition, the numerical investigations of incompressible Newtonian flows on the structure of the incompressible through a channel have been widely conducted compared to (see for example [12]). In contrast, one can see that a few numerical studies related to compressible axisymmetric flows past a channel have been introduced due to the extreme difficulties. Thus this study is concerned with the investigation of this type of flows.

The main difficulty in developing a numerical algorithm to treat the compressible flows comes from that the differential equations turn to a hyperbolic-parabolic system, while those for incompressible flow are an elliptic-parabolic. In addition, the compressible equations for low Mach number may be associated with large disparity between the acoustic wave-speed, (u + c), and the entropy wave convected at the fluid-speed, (u) [13-15]. Here, the condition number for the equation system is related to the reciprocal of the Mach number.

The present study aims to present a study on the compressible Newtonian fluid with a constant viscosity. The novelty here is to study the temporal convergence-rate of the system solution that is taken to be steady state, compressible, axisymmetric, and laminar, which did not address by researchers previously. In this context, Poiseuille(Ps) flow along a two dimensional planar straight channel, under isothermal condition is studied. The main results of current study focused comparison against incompressible counterparts in the temporal convergence rates for the components of the solution. Furthermore, the rate of covergence for three different meshes are compared. Numerical treatments are presented for governing system, where we have utilized the Galerkin finite element. The unequal order primitive variable of velocity components and pressure will be employed as the main approach. For the numerical solution, the iterative method of Newton-Raphson will be used to solve the set of non-linear equations and the backward different scheme will be employed as the time-integration approach to deal with the time dependent term. In the next section, the governing equations of the Newtonian flows are introduced in the cylindrical coordinates. Since these equations must be studied numerically, the numerical method is characterized in Section 3. The problem discretisation and the related numerical results are presented in Section 4 and 5, respectively.

2. Mathematical modeling

The dimensionless form of continuity and momentum equations of compressible Newtonian flow under isothermal condition and omitting the body forces can be given in cylindrical coordinates as:

$$\frac{\partial \rho}{\partial t}+\frac{1}{r}\frac{\partial}{\partial r}(\rho r u_r)+\frac{1}{r}\frac{\partial}{\partial \theta}(\rho u_\theta)+\frac{\partial}{\partial z}(\rho u_z)=0. \quad (1)$$

r-direction

$$\rho\left(\frac{\partial U_r}{\partial t}+U_r\frac{\partial U_r}{\partial r}+\frac{U_\theta}{r}\frac{\partial U_r}{\partial \theta}+U_z\frac{\partial U_r}{\partial z}-\frac{U_\theta U_\theta}{r}\right)$$

$$=-\frac{\partial p}{\partial r}+\frac{4\mu}{3}\frac{\partial^2 U_r}{\partial r^2}+\frac{4\mu}{3r}\frac{\partial U_r}{\partial r}-\frac{4\mu}{3r^2}U_r+\frac{\mu}{3r}\frac{\partial^2 U_\theta}{\partial r\partial\theta}-\frac{4\mu}{3r^2}\frac{\partial U_\theta}{\partial \theta}$$

$$+\frac{\mu}{r^2}\frac{\partial^2 U_r}{\partial \theta^2}+\mu\frac{\partial^2 U_r}{\partial z^2}+\frac{\mu}{3}\frac{\partial^2 U_z}{\partial r\partial z}-\frac{\mu}{r^2}\frac{\partial U_r}{\partial r} \quad (2)$$

θ-direction

$$\rho\left(\frac{\partial U_\theta}{\partial t}+U_r\frac{\partial U_\theta}{\partial r}+\frac{U_\theta}{r}\frac{\partial U_\theta}{\partial \theta}+U_z\frac{\partial U_\theta}{\partial z}+\frac{\partial U_r U_\theta}{r}\right)$$

$$=-\frac{1}{r}\frac{\partial p}{\partial \theta}+\frac{\mu}{3r}\frac{\partial^2 U_r}{\partial r\partial\theta}+\frac{7\mu}{3r^2}\frac{\partial U_r}{\partial \theta}+\frac{4\mu}{3r^2}\frac{\partial^2 U_\theta}{\partial \theta^2}$$

$$+\frac{\mu}{3r}\frac{\partial^2 U_z}{\partial\theta\partial z}+\mu\frac{\partial^2 u_\theta}{\partial z^2}+\mu\frac{\partial^2 u_\theta}{\partial r^2}+\frac{\mu}{r}\frac{\partial U_\theta}{\partial r}-\frac{\mu}{r^2}U_\theta \quad (3)$$

z-direction

$$\rho\left(\frac{\partial U_z}{\partial t}+U_r\frac{\partial U_z}{\partial r}+\frac{U_\theta}{r}\frac{\partial U_z}{\partial \theta}+U_z\frac{\partial U_z}{\partial z}\right)$$

$$=-\frac{\partial p}{\partial z}-\frac{2\mu}{3}\frac{\partial^2 U_r}{\partial r\partial z}+\frac{\mu}{3r}\frac{\partial U_r}{\partial z}+\frac{\mu}{3r}\frac{\partial^2 U_\theta}{\partial\theta\partial z}+\frac{4\mu}{3}\frac{\partial^2 U_z}{\partial z^2}$$

$$+\mu\frac{\partial^2 U_z}{\partial r^2}+\mu\frac{\partial^2 U_z}{\partial r\partial z}+\frac{\mu}{r^2}\frac{\partial^2 U_z}{\partial \theta^2}+\frac{\mu}{r}\frac{\partial U_z}{\partial r} \quad (4)$$

Where, u_r, u_θ and u_z are the velocity components in r-direction, θ-direction and z-direction, respectively, p is the pressure and ρ is the fluid density (for more details see [16-22]).

3. Numerical method

In this study, Galerkin finite element method (GFEM) is used to solve the related governing equations (2)-(4). This approach begins with finding the weak form of the continuity and momentum equations by using appropriate weight functions, then integrating over a typical domain and substituting assumed approximate solutions, to get the the following matrix form

$$[M][U_r] + [C_r(U_r)][U_r] + [C_z(U_z)][U_r] - [C_\theta][U_\theta] - [Q_r][\rho] + \frac{4}{3}[K_{r_r}] + \frac{4}{3}[K_r][U_r] + \frac{4}{3}[q_r][U_r] + [K_{z_z}][U_r] + \frac{1}{3}[K_{r_z}][U_z] = [0] \quad (5)$$

$$[M][U_\theta] + [C_r(U_r)][U_\theta] + [C_z(U_z)][U_\theta] - [C_r][U_\theta] + [K_{z_z}][U_\theta] + [K_{r_r}][U_\theta] + [K_r][U_\theta] + [q_\theta][U_\theta] = [0] \quad (6)$$

$$[M][U_z] + [C_r(U_r)][U_z] + [C_z(U_z)][U_z] - [Q_z][\rho] - \frac{2}{3}[K_{rz}][U_r] + \frac{1}{3}[K_z][U_r] + \frac{4}{3}[K_{z_z}][U_z] + [K_{r_r}][U_z] + [K_{r_z}][U_z] + [K_r][U_z] = [0] \quad (7)$$

$$[M\rho][\rho\cdot] + [Q_1][U_r] + [q_1][\rho] + [S][U_r] + [Q_2][U_\forall] + [q_2][\rho] + [Q_3][U_z] + [q_3][\rho] = [0] \quad (8)$$

where,

$$[Q] = [C_r(U_r)] + [C_\theta(U_\theta)] + [C_z(U_z)] + [Q_r] + [Q_\theta] + [Q_z] + [K_{22}] + [K_r] + [K_{rr}] + [K_{zz}]$$

Here, the quadratic shape functions that proposed for velocity components can be defined as:

$$\begin{bmatrix}\psi_1\\ \psi_2\\ \psi_3\\ \psi_4\\ \psi_5\\ \psi_6\end{bmatrix} = \begin{bmatrix}L_1^2 - L_1L_2 - L_1L_3\\ L_2^2 - L_2L_3 - L_2L_1\\ L_3^2 - L_3L_1 - L_3L_2\\ 4L_1L_2\\ 4L_2L_3\\ 4L_3L_1\end{bmatrix} = \begin{bmatrix}1 & 0 & 0 & -1 & 0 & -1\\ 0 & 1 & 0 & -1 & -1 & 0\\ 0 & 0 & 1 & 0 & -1 & -1\\ 0 & 0 & 0 & 4 & 0 & 0\\ 0 & 0 & 0 & 0 & 4 & 0\\ 0 & 0 & 0 & 0 & 0 & 4\end{bmatrix}\begin{bmatrix}L_1^2\\ L_2^2\\ L_3^2\\ L_1L_2\\ L_2L_3\\ L_1L_3\end{bmatrix}. \quad (9)$$

In contrast, a convenient linear shape function is proposed for pressure and density, such that

$$\begin{bmatrix}\phi_1\\ \phi_2\\ \phi_3\end{bmatrix} = \begin{bmatrix}L_1\\ L_2\\ L_3\end{bmatrix}. \quad (10)$$

where, L_1, L_2, and L_3 are local triangular coordinates.

Correspondingly, we can dfine the matrices of the above system as follows:

The mass matrix is given by:

$$[T] = 2\pi r_m A[K][M][M^T][K^T].$$

And the convective matrices can be expressed as:

$$[Y_r(U_r)] = 2\pi r_m A[K][M][M^T][K^T][U_r][N^T][B^T][K^T] .$$

$$[Y_\theta(U_\theta)] = [0] .$$

$$[Y_z(U_z)] = 2\pi r_m A[K][M][M^T][K^T][U_z][N^T][C^T][K^T] .$$

$$[S_r(U_r)] = 2\pi A[K][M][M^T][K^T][U_r][M^T][K^T] .$$

$$[S_\theta(U_\theta)] = -2\pi A[K][M][M^T][K^T][U_\theta][M^T][K^T].$$

Also, the diffusion matrices are gathered as:

$$[H_r] = 2\pi r_m A \frac{1}{Re}[K][B][N][N^T][B^T][K^T]$$

$$[H_\theta] = [0]$$

$$[H_z] = 2\pi r_m A \frac{1}{Re}[K][C][N][N^T][C^T][K^T]$$

$$[D_r] = -2\pi A \frac{1}{Re}[K][M][N^T][B^T][K^T]$$

$$[D_\theta] = [0]$$

$$[T_a] = 2\pi \frac{1}{r_m} A \frac{1}{Re}[K][M][M^T][K^T].$$

The gradient matrices are given by:

$$[F_r] = 2\pi r_m A[K][B][N][N^T]$$

$$[F_\theta] = [0]$$

$$[F_z] = 2\pi r_m A[K][C][N][N^T]$$

$$[F_a] = 2\pi A[N][M^T][K^T]$$

$$[E_\rho] = \begin{bmatrix} J_1 \\ J_2 \\ J_3 \end{bmatrix}, \ [B_\rho] = \frac{1}{2A}\begin{bmatrix} b_1 \\ b_2 \\ b_3 \end{bmatrix}, \ [C_\rho] = \frac{1}{2A}\begin{bmatrix} C_1 \\ C_2 \\ C_3 \end{bmatrix},$$

where, A is the area of the triangular element and $r_m = \frac{1}{3}(r_1 + r_2 + r_3)$,

and

$$[K] = \begin{bmatrix} 1 & 0 & 0 & -1 & 0 & -1 \\ 0 & 1 & 0 & -1 & -1 & 0 \\ 0 & 0 & 1 & 0 & -1 & -1 \\ 0 & 0 & 0 & 4 & 0 & 0 \\ 0 & 0 & 0 & 0 & 4 & 0 \\ 0 & 0 & 0 & 0 & 0 & 4 \end{bmatrix} \cdot [M] = \begin{bmatrix} L_1^2 \\ L_2^2 \\ L_3^2 \\ L_1 L_2 \\ L_2 L_3 \\ L_1 L_3 \end{bmatrix} \quad [N] = \begin{bmatrix} L_1 \\ L_2 \\ L_3 \end{bmatrix}$$

$$[B] = \frac{1}{2A}\begin{bmatrix} 2\beta_1 & 0 & 0 \\ 0 & 2\beta_2 & 0 \\ 0 & 0 & 2\beta_3 \\ \beta_2 & \beta_1 & 0 \\ 0 & \beta_3 & \beta_2 \\ \beta_3 & 0 & \beta_1 \end{bmatrix} \cdot [C] = \frac{1}{2A}\begin{bmatrix} 2\gamma_1 & 0 & 0 \\ 0 & 2\gamma_2 & 0 \\ 0 & 0 & 2\gamma_3 \\ \gamma_2 & \gamma_1 & 0 \\ 0 & \gamma_3 & \gamma_2 \\ \gamma_3 & 0 & \gamma_1 \end{bmatrix}$$

such that β_i and γ_j . i . $j = 1$ .2 .3 are coefficients defined in terms of coordinates of triangular element. In addition, to complete the numerical building the Newton-Raphson method has been used to address the nonlinear part based on the system backward Euler scheme (see [23,24]). In this context, the system of equations is given by:

$$[T][\dot{U}_r] + [\frac{\partial R_1}{\partial U_r}][\Delta U_r] + [\frac{\partial R_1}{\partial U_\theta}][\Delta U_\theta] + [\frac{\partial R_1}{\partial U_z}][\Delta U_z] + [\frac{\partial R_1}{\partial P}][\Delta P] + [\frac{\partial R_1}{\partial \rho}][\Delta \rho] = -[R_1] \quad (11)$$

$$[T][\dot{U}_\theta] + [\frac{\partial R_2}{\partial U_r}][\Delta U_r] + [\frac{\partial R_2}{\partial U_\theta}][\Delta U_\theta] + [\frac{\partial R_2}{\partial U_z}][\Delta U_z] + [\frac{\partial R_2}{\partial P}][\Delta P] + [\frac{\partial R_2}{\partial \rho}][\Delta \rho] = -[R_2] \quad (12)$$

$$[T][\dot{U}_z] + [\frac{\partial R_3}{\partial U_r}][\Delta U_r] + [\frac{\partial R_3}{\partial U_\theta}][\Delta U_\theta] + [\frac{\partial R_3}{\partial U_z}][\Delta U_z] + [\frac{\partial R_3}{\partial P}][\Delta P] + [\frac{\partial R_3}{\partial \rho}][\Delta \rho] = -[R_3] \quad (13)$$

$$[T][\dot{P}] + [\frac{\partial R_4}{\partial U_r}][\Delta U_r] + [\frac{\partial R_4}{\partial U_\theta}][\Delta U_\theta] + [\frac{\partial R_4}{\partial U_z}][\Delta U_z] + [\frac{\partial R_4}{\partial P}][\Delta P] + [\frac{\partial R_4}{\partial \rho}][\Delta \rho] = -[R_4] \quad (14)$$

Where,

$$R_1 = [C_r(U_r)][U_r] + [C_z(U_z)][U_r] + \frac{4}{3}[K_{rr}][U_r] + \frac{4}{3}[K_r][U_r] + \frac{4}{3}[q_r]$$

$$[U_r] + [K_{rr}][U_r] + [C_\theta][U_\theta] + \frac{1}{3}[K_{rz}][U_z] - [Q_r][P] \quad (15)$$

$$R_2 = [C_r(U_r)][U_\theta] + [C_z(U_z)][U_\theta] + [C_r][U_\theta] + [K_{zz}][U_\theta] + [K_{rr}]$$

$$[U_\theta] + [K_r][U_\theta] + [q_r][U_\theta] \quad (16)$$

$$R_3 = -\frac{2}{3}[K_{rz}][U_r] + \frac{1}{3}[K_z][U_r] + [C_r(U_r)][U_z] + [C_z(U_z)][U_z] +$$

$$[C_z(U_z)][U_z] + \tfrac{4}{3}[K_{zz}][U_z] + [K_{rr}][U_z] + [K_{rz}][U_z] + [K_r][U_z] - [Q_z][P] \quad (17)$$

$$R_4 = [Q_1][U_r] + [S][U_r] + [Q_3][U_z] + [q_1][\rho] + [q_3][\rho] \quad (18)$$

such that, $[Q]$ is reduced to the form:

$$[Q] = [C_r(U_r)] + [C_\theta(U_\theta)] + [C_z(U_z)] + [Q_r] + [Q_\theta] + [Q_z]$$

$$+[K_{22}] + [K_r] + [K_{rr}] + [K_{zz}] \quad (19)$$

4. Problem discretization

In this article, the problem of the flow is selected to be a 2D channel connected to upstream and downstream cylinders. In this context, a Poiseuille flow through a 2D-axisymmetric channel considered, for an isothermal, compressible Newtonian fluid. Three finite element meshes, $M_1 = 10 \times 10$, $M_2 = 20 \times 20$ and $M_3 = 30 \times 30$ are used for this purpose (see Figure1(a),(b),(c)). The results are shown for tolerance criteria taken as $TOL = 10^{-10}$ and typical Δt is $O(10^{-3})$. Mesh characteristics are introduced in Table 1.

Table 1: Characteristics of the achieved meshes.

Mash	Total Element	Total Nodes	Boundary Nodes	Pressure Nodes
M_1=10×10	200	441	80	40
M_2=20×20	800	1681	160	80
M_3=30×30	1800	3721	240	120

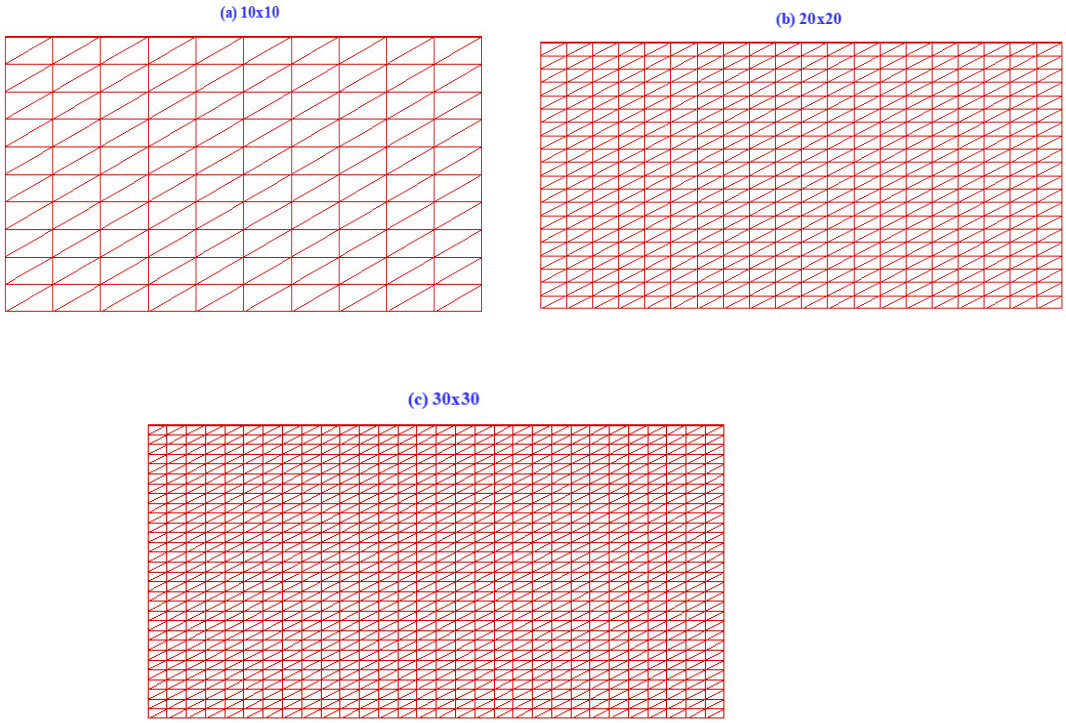

Figure 1: Structured (a) 10x10, (b) 20x20 and (c) 30x30 finite element meshes.

Boundary conditions (BCs):

The BCs of the present problem can be define as (see Figure 2):

The setting of BCs of the present channel problem is laid as follows (see Figure 2):

1. Zero radial velocity is applied at the inlet, outlet and centerline of the channel.
2. Poiseuille(Ps) flow is applied at the inlet.
3. Along with the outflow, zero pressure is applied.

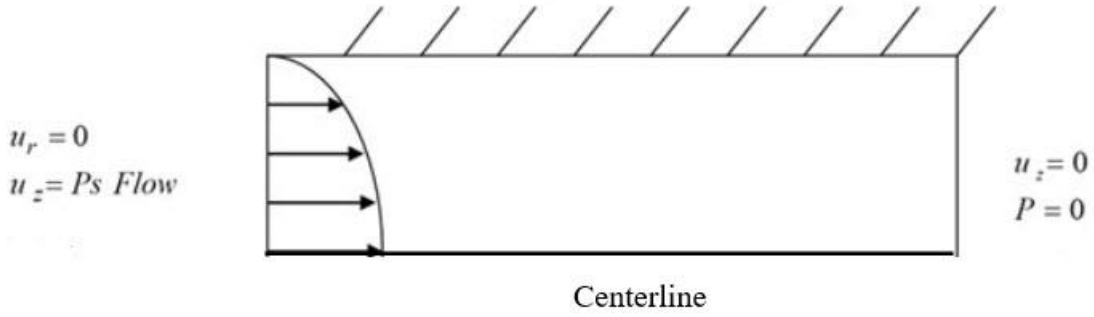

Figure 2: Schema for flow problem and boundary conditions.

5. Numerical results

The numerical results concerned with the rate of convergence of the problem under consideration by using a Galerkin finite element method. The rate of convergence for axial velocity and pressure components for compressible and incompressible cases are presented in Figures 3 and 4 based on three different meshes and *Re*=1. From the findings, one can see that for both cases there is clear differences in the level of convergence of velocity for the three meshes (see Figure 3). In addition, the velocity convergence in a compressible fluids is higher than its counterpart in an incompressible.

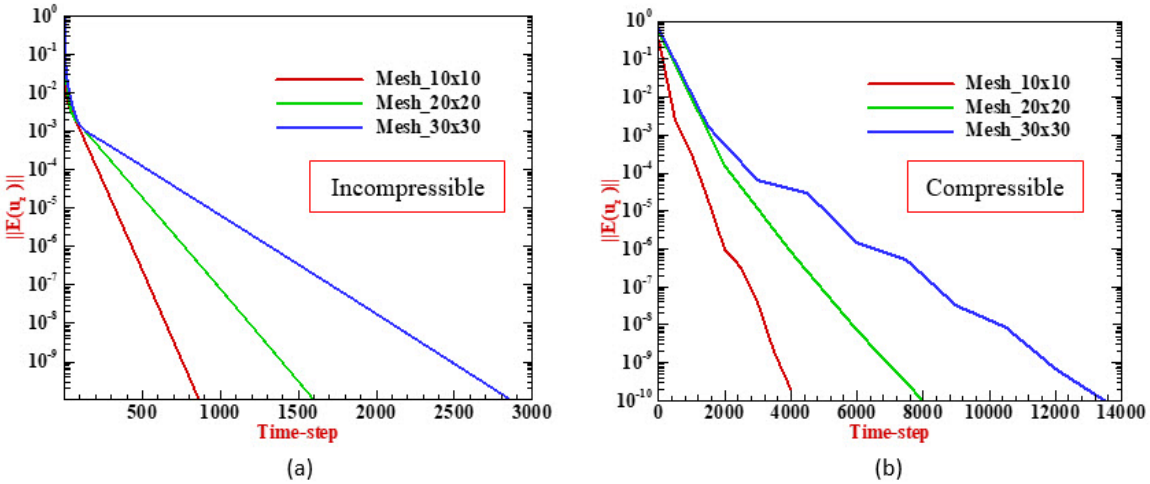

Figure 3: Convergence of velocity; (a) Incompressible, (b) compressible variation, Re=1.

Again the pressure convergence is provided in Figures 4 for both compressible and incompressible cases based on three various meshes and *Re*=1. Here, the same featuere of velocity convergence is observed in the pressure case. There, in both situations with a higher level of convergence in a compressible as compare with an incompressible as well.

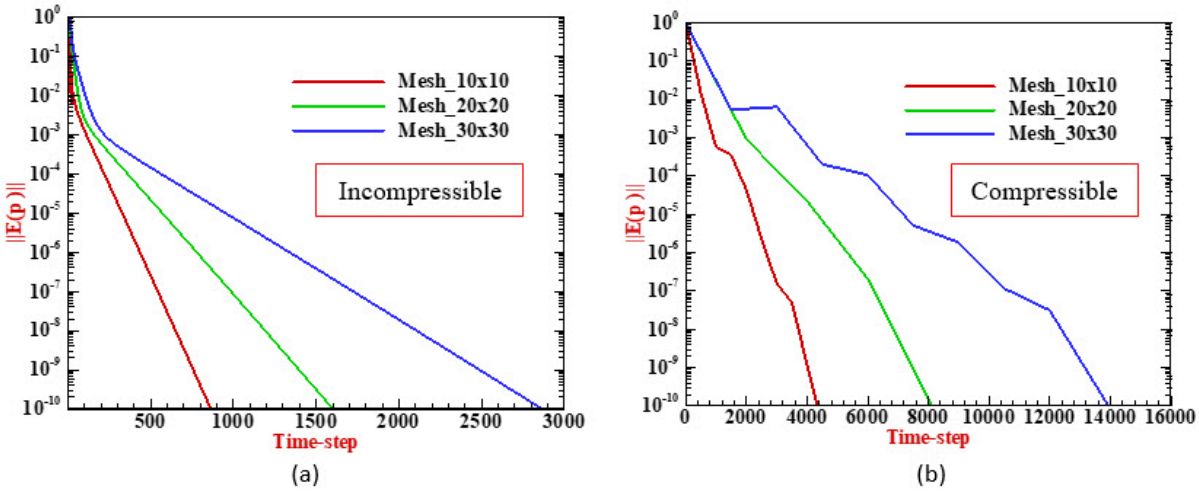

Figure 4: Convergence of pressure; (a) Incompressible, (b) compressible variation, Re=1.

The axial velocity and pressure drop profiles through the centerline are presented in Figure 5 for fine mesh in both incompressible and compressible instances and *Re*=1. The findings reveal that, the level of velocity is higher in the compressible case as compared to that for the incompressible situation. Same behaviour in pressure is observed, where the maximum level of pressure of around 16 units is detected in the compressible case at the inlet of the channel (see Figure 5b). Also, more details about the solution components are presented in Table 2.

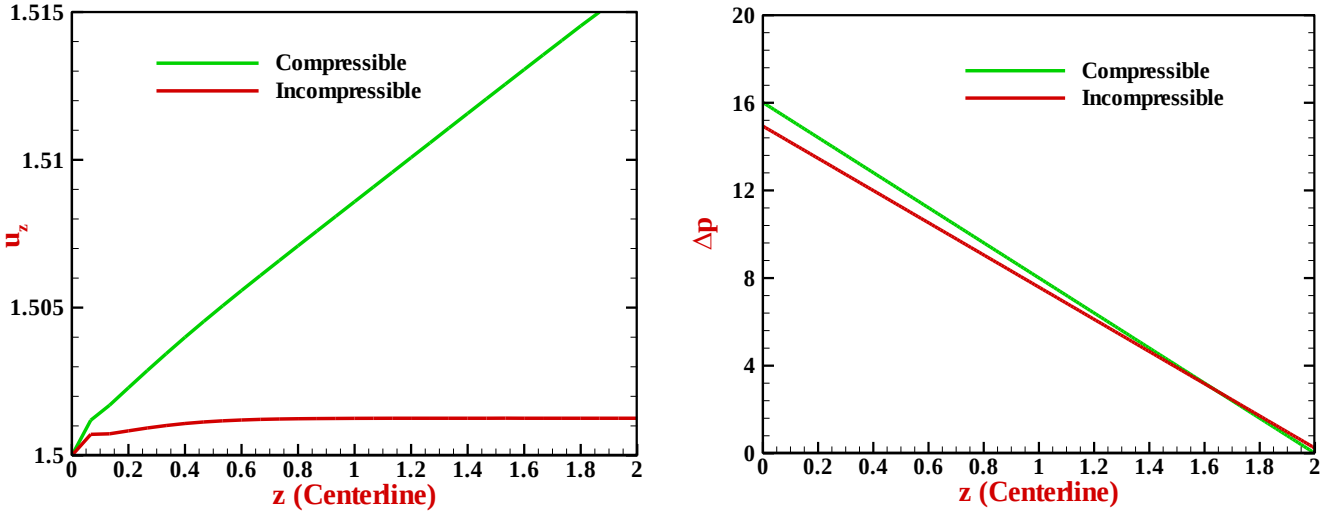

Figure 5: Comparison between Incompressible and compressible solutions along centerline; (a) axial velocity, (b) pressure drop, Re=1, fine mesh (M_3)

Table 2: Maximum value: velocity and pressure; Re-variation

Maximum value	Incompressible			Compressible		
	Re=1	Re=5	Re=10	Re=1	Re=5	Re=10
u_z	2.00168	2.00168	2.00168	2.01702	2.02737	2.03702
u_r	0.00002	0.00003	0.00005	0.000102	0.00013	0.00017
p	16.1946	16.1977	16.1978	16.2478	16.2678	16.2924

Moreover, the results for density and Mach number are presented in Figure 6(a,b) for fine mesh in compressible instances with *Re*=1. The profile shows a linear decline in density occurs throughout the channel, after which the density reduction to zero. An opposite feature is observed in Mach number behaviour throughout the channel, where a sharp increase is occurred to reach the maximum level of around 0.0505 units at the outlet of the channel. Thus, from the low level of Mach number one can conclude that, the ability of the weakly-compressible

implementations. In addition, the low range of Mach number ((0.0492<Ma<0.0506) demonstrate that, the piecewise-constant density interpolation is equitable to linear density interpolation. So we can say that, our algorithm employ effectively to simulate weakly-compressible. Density is plotted as a function of Mach number in Figure 6c. The results show that, a linear related is formed between the density and Mach number.

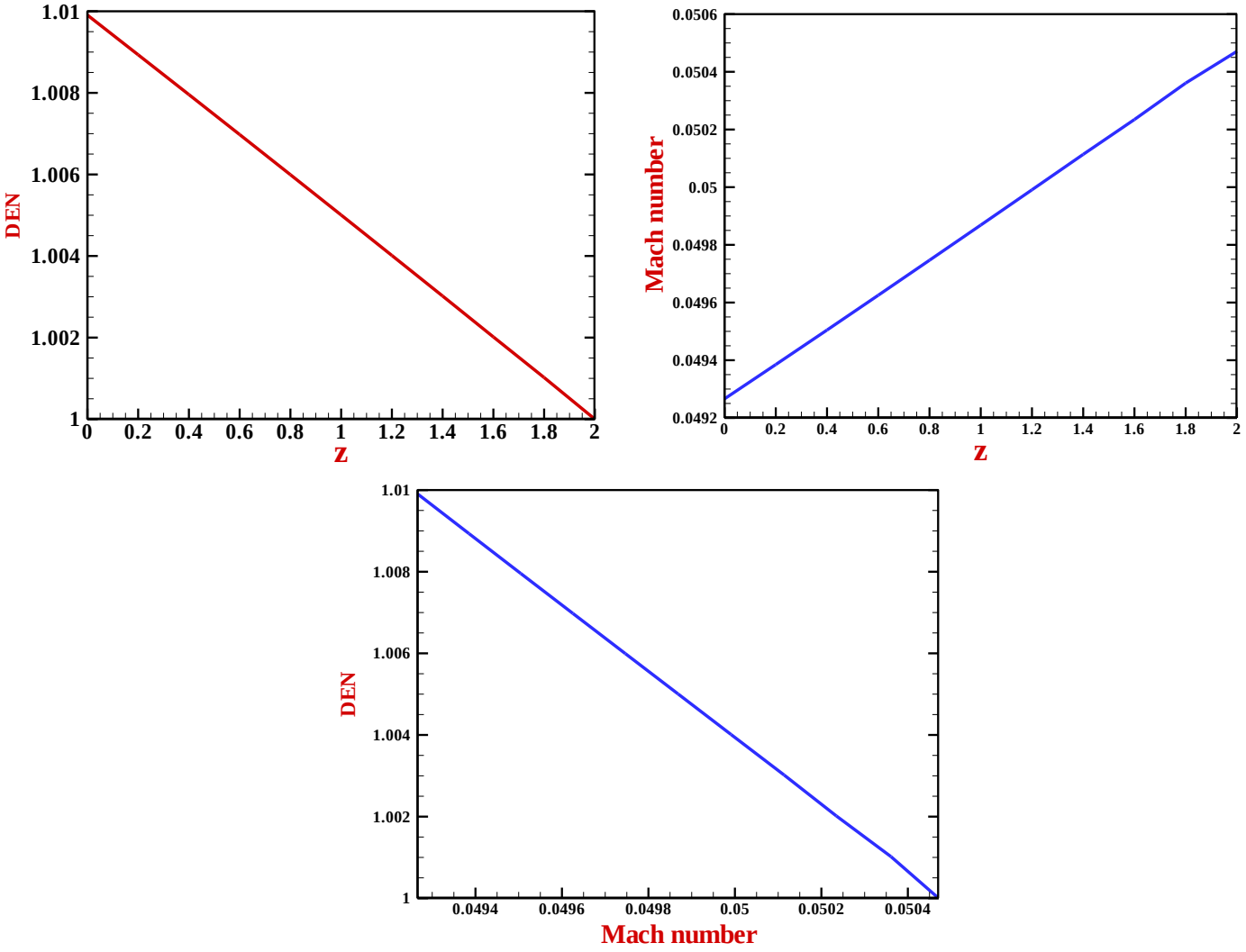

Figure 6: (a) density, (b) mach number, (c) density as a function of mach number; Re=1, fine mesh (M_3)

6. Conclusion

In this paper, the numerical simulation for compressible Newtonian fluid is achieved based on the Galerkin finite element method in a cylindrical coordinates system. Simultaneously to treat the non-linear equations, the Newton-Raphson iterative method based on backward difference scheme is employed as well. For that purpose three finite element meshes are utilized. The

convergence analysis of velocity and pressure was done for both compressible and incompressible cases. In this context, the results reveal that, the rate of convergence for compressible flow is higher thane incompressible for both velocity and pressure solutions. In addition, the level of Mach number and that relationship with the density has been studied. Consequently, the results show that the low level of Mach number gives a constant density, which this in experimental results and with what the other findings.

References

[1] R. B. Bird, W. E. Stewart, E. N. Lightfoot, Transport Phenomena, John Wiley and Sons, New York, NY, 2nd edition, 2002.

[2] A.S.J.Al-Saif, Numerical study for convection motion stability of the incompressible two-dimensional fluid flow by DQM. J Bas Res. Sci, 33 (2007)70-80

[3] K.H.Becker,Understanding Rheology, An Introduction to Rheology,Springer International Publishing, Cham, Switzerland, 2017.

[4] G.Haukea,T.J.R. Hughesb, A comparative study of different sets of variables for solving compressible and incompressible flows, Comput. Methods Appl. Mech. Eng.,153 (1998)1-44.

[5] M.A.Kelmanson, S.B.Maunder, Modelling high velocity impact phenomena using unstructured dynamically adaptive Eulerian meshes, J Mech. Phys. Solids, 4 (1999) 731-762.

[6] Y.Wu, K.Pruess, Integral solutions for transient fluid flow through a porous medium with pressure dependent permeability, Int. J. Rock Mech. Min., 37(2000) 51-61.

[7] T. Papanastasiou, G.Georgios, N.A Andreas,Viscous fluid flow, CRC press, 2021.

[8] K.H.Han, Y.T.IM,Compressible flow analysis of filling and post-filling in injection molding with phase-change effect, Compos. Struct., 1(1997)179-190.

[9] M.Ranganathan, M.R.Mackley, P.H.J.Spitteler,The application of the multipass Rheometer to time dependent capillary flow measurements of a Polyethylene melt, J Rheol, 2 (1999)443-451.

[10] M. F.Webster, I. J. Keshtiban, F. Belblidia,Computation of Weakly-Compressible Highly-Viscous Polymeric Liquid Flows, Eng Comput,7(2004)777-804.

[11] T.J.R. Hughes, L.P. Franca, G.M. Hulbert, A new finite element formulation for computational fluid dynamics: VIII. The Galerkin Least-Squares method for advectivediffusive equations, Computer Methods in Applied Mechanics and Engineering, 73(1989)173–189.

[12] R.Manica, A.Bortoli, Simulation of Incompressible Non-Newtonian Flows Through Channels with Sudden Expansion Using the Power Law Model1, TEMA Soc. Bras. Mat. Apl. Comput., 4(2003)333-340.

[13] J.S.Wong, D.L.Darmofal, J. Peraire,The solution of the compressible Euler equations at low Mach numbers using a stabilized finite element algorithm ,Computer Methods in Applied Mechanics and Engineering,190(2001)5719-5737.

[14] E. Turkel, R. Radespiel, N.Kroll, Assessment of preconditioning methods for ultidimensional aerodynamics, Comput. Fluids., 6(1997)613-634.

[15] P. Jennyand, B. Muller, Convergence acceleration for computing steady-state compressible flow at low Mach numbers, Comput. Fluids., 8(1999)951-972.

[16] A.N. Abdulhasan, and A.H. Al-Muslimawi, Numerical investigation of extensional flow through axisymmetric conical geometries: Finite element method. Bas. J. Sci., 38(2020)399-421.

[17] A. Al-Muslimawi, H.R. Tamaddon-Jahromi, M. F. Webster, Numerical simulation of tube-tooling cable-coating with polymer melts, Korea Aust. Rheol. J., 25 (2013) 197-216.

[18] J. E. Lopez-Aguilar, M. F. Webster, A. H. A. Al-Muslimawi, H. R. Tamaddon-Jahromi, R. Williams, K. Hawkins, C. Askill, C. L. Ch'ng, G. Davies, P. Ebden, K. Lewis, A computational extensional rheology study of two biofluid systems, Rheol Acta., 54 (2015) 287-305.

[19]] A. H. Al-Muslimawi, Taylor Galerkin Pressure Correction (TGPC) Finite Element Method for Incompressible Newtonian Cable-Coating Flows, J Kufa Math. Comput, 5 (2018)13-21.

[20] R.Y. Yasir, A.H. Al-Muslimawi, B.K. Jassim, Numerical simulation of non-Newtonian inelastic flows in channel based on artificial compressibility method, J. Appl. Comput. Mech.,6(2020)271-283.

[21] A.Al-Muslimawi,H.R.Tamaddon-Jahromi, M.F.Webster, Numerical simulation of tube tooling cable-coating with polymer melts, Korea Aust. Rheol. J., 25(2013)197 -213.

[22] A.M. Jasim, and A.J. Al-Maliki, New Analytical Study of Non-Newtonian Jeffery Hamel Flow of Casson Fluid in Divergent and Convergent Channels by Perturbation Iteration Algorithm, Bas. J Sci.,39(2021)37-55.

[23] R.Y. Yasir, A.H.Al-Muslimawi, Numerical simulation of Power-Law inelastic fluid in channal by using finite element method. Bas. J. Sci., 37(2019)163-180.

[24] I.A. Fadhel, and A.H.Al-Muslimawi, Simulation of Newtonian axisymmetric pipe flow by using a Taylor Galerkin/pressure correction finite element method , Bas. J. Sci. ,38(2020)198-222.

تطوير خوارزمية لتدفق السوائل الانضغاطية النيوتونية الاعتماد على طريقة العناصر المحدودة

فاطمة عبد الرزاق ، علاء المسلماوي ، ريسان ياسين ياسر

قسم الرياضيات ، كلية العلوم ، جامعة البصرة ، البصرة، العراق

المستخلص

في هذه المقالة ، قدمنا دراسة عددي لتدفق نيوتن مضغوط في قناة ثنائية الأبعاد متناظرة. طريقة Galerkin للعناصر المحدودة تم تطبيقها لاستيعاب التدفقات القابلة للضغط وغير القابلة للضغط. معادلة الاستمرارية والحفظ المعتمد على الوقت لمعادلات الزخم تُستخدم لوصف حركة المائع ، والتي يتم الحفاظ عليها في نظام الإحداثيات الأسطواني (تناظر المحور). الحقيق تحليل الطريقة ، يتم استخدام تدفق Poiseuille على طول قناة دائرية تحت حالة متساوي الحرارة كمشكلة اختبار بسيطة. هذا الاختبار يتم إجرائه بأخذ مقطع دائري من الأنبوب. مقارنة بين النتائج القابلة للضغط وغير القابلة للضغط في درجات التقارب للسرعة والضغط المحوريين تم إجرائها. تكشف النتائج أن معدلات تقارب السرعة والضغط تكون أسرع في حالة غير قابلة للضغط مقارنةً بالضغط. بالإضافة إلى ذلك ، فإن مستوى تقارب السرعة أعلى من الضغط لكل من حالة الانضغاط وغير القابل للضغط. علاوة على ذلك ، فإن المستوى المنخفض لرقم ماخ يوضح أن الاستيفاء متعدد التعريف للكثافة يكون مساويًا لاستيفاء الكثافة الخطية.